Histone H3 lysine 9 di-methylation as an epigenetic signature of the interferon response

Terry C. Fang,[1] Uwe Schaefer,[1] Ingrid Mecklenbrauker,[1] Astrid Stienen,[1,5] Scott Dewell,[3] Marie S. Chen,[1] Inmaculada Rioja,[4] Valentino Parravicini,[4] Rab K. Prinjha,[4] Rohit Chandwani,[1] Margaret R. MacDonald,[2] Kevin Lee,[4] Charles M. Rice,[2] and Alexander Tarakhovsky[1]

[1]Laboratory of Immune Cell Epigenetics and Signaling, [2]Laboratory of Virology and Infectious Disease, and [3]Genomics Resource Center, Rockefeller University, New York, NY 10065
[4]Epinova DPU, Immuno-Inflammation Centre of Excellence for Drug Discovery, GlaxoSmithKline, Medicines Research Centre, Stevenage SG1 2NY, England, UK
[5]Department of Pediatrics, UK Aachen, University Hospital RWTH, 52074 Aachen, Germany

Effective antiviral immunity depends on the ability of infected cells or cells triggered with virus-derived nucleic acids to produce type I interferon (IFN), which activates transcription of numerous antiviral genes. However, disproportionately strong or chronic IFN expression is a common cause of inflammatory and autoimmune diseases. We describe an epigenetic mechanism that determines cell type–specific differences in IFN and IFN-stimulated gene (ISG) expression in response to exogenous signals. We identify di-methylation of histone H3 at lysine 9 (H3K9me2) as a suppressor of IFN and IFN-inducible antiviral gene expression. We show that levels of H3K9me2 at IFN and ISG correlate inversely with the scope and amplitude of IFN and ISG expression in fibroblasts and dendritic cells. Accordingly, genetic ablation or pharmacological inactivation of lysine methyltransferase G9a, which is essential for the generation of H3K9me2, resulted in phenotypic conversion of fibroblasts into highly potent IFN-producing cells and rendered these cells resistant to pathogenic RNA viruses. In summary, our studies implicate H3K9me2 and enzymes controlling its abundance as key regulators of innate antiviral immunity.

CORRESPONDENCE
Terry C. Fang:
tfang@rockefeller.edu
OR
Alexander Tarakhovsky:
tarakho@rockefeller.edu

Abbreviation used: ISG, IFN-stimulated gene; MEF, mouse embryonic fibroblast; VSV, vesicular stomatitis virus.

Type I IFN (IFN-α/β) is a potent proinflammatory cytokine that facilitates innate and adaptive immune responses against viruses and bacterial pathogens (Stetson and Medzhitov, 2006). The proinflammatory potential of IFN-α/β (hereafter defined as IFN) implies the necessity for tight control of this cytokine expression. In the absence of a clinically manifested infection, IFN levels in the organism are largely supported by plasmacytoid DCs (Barchet et al., 2005), which are characterized by exceptionally high spontaneous or signal-induced IFN production. Heightened IFN production by plasmacytoid DCs reflects an overall potent capacity of the innate immune cells, such as macrophages, DCs, and monocytes, to transcribe IFN and IFN-stimulated genes (ISGs) in response to pathogens or pathogen-derived ligands (Diebold et al., 2003; Pietras et al., 2006; Kumagai et al., 2007). In contrast to cells of the innate immune system, parenchymal cells, as well as neurons and cardiac myocytes, must exert tight control over IFN expression to avoid tissue injury (Trinchieri, 2010).

The mechanism of cell type–specific differences in IFN expression is not well understood. Expression of IFN genes, which include a single *Ifnβ* and multiple *Ifnα* genes, is determined at two different levels. First, the activity of signaling proteins downstream of pathogen-sensing receptors triggers nuclear translocation of transcription factors that activate *Ifnα/β* gene expression. Studies of *Ifnβ* gene transcription show that binding of viral and synthetic nucleic acid to their respective receptors initiates a signaling cascade that leads to nuclear

The Rockefeller University Press $30.00
J. Exp. Med. Vol. 209 No. 4 661-669
www.jem.org/cgi/doi/10.1084/jem.20112343

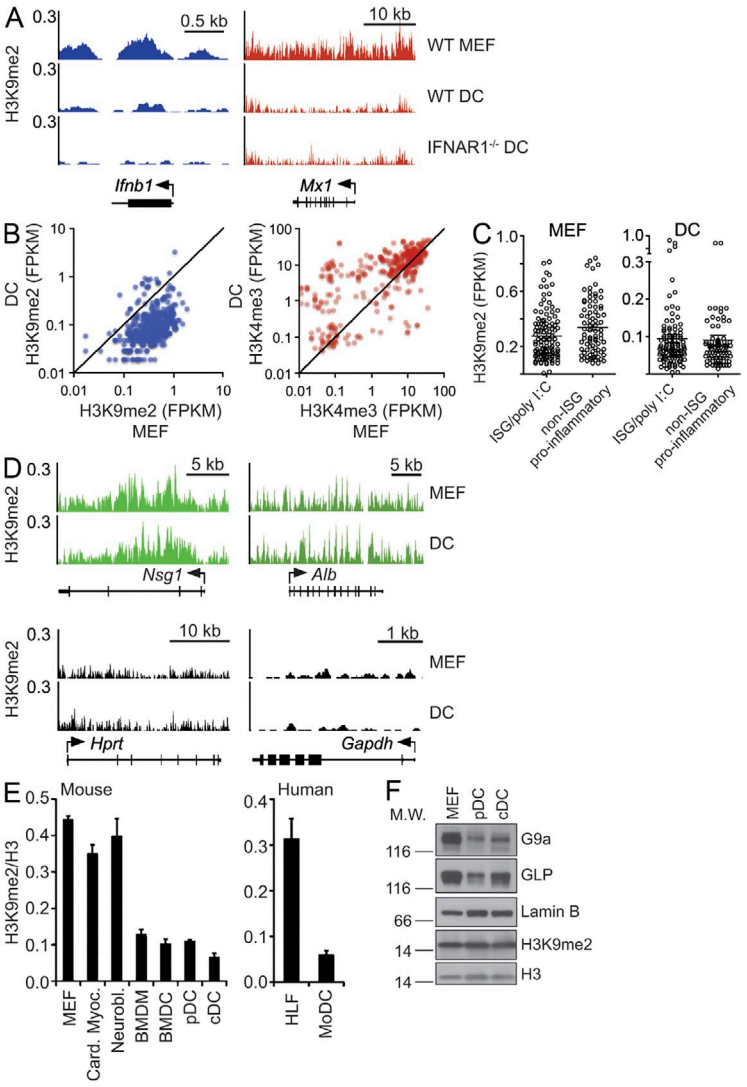

Figure 1. Diminished H3K9me2 at IFN and IFN-inducible genes (ISGs) in DCs compared with MEFs. (A) H3K9me2 levels and distribution at the *Ifnb1* and *Mx1* gene loci in WT MEFs and in splenic DCs from WT and IFNAR1$^{-/-}$ mice. The gene fragments associated with H3K9me2 were identified and quantified by ChIP-Seq analysis. Y-axes represent the number of reads per million mapped reads per 25 bp window. (B) Scatter plots display relative FPKM (fragments per kb per million mapped reads) values of H3K9me2 or H3K4me3 for individual ISGs in WT MEFs (x-axes) and splenic DCs (y-axes). ChIP-Seq represents three independent experiments for MEFs and two experiments for DCs. (C) Abundance of H3K9me2 at ISGs and poly I:C–inducible genes and non-ISG proinflammatory genes in MEFs and DCs. FPKM values of H3K9me2 for ISGs in WT MEFs (left) and splenic DCs (right). ChIP-Seq represents three independent experiments for MEFs and two experiments for DCs. The horizontal bars represent the mean ± SEM. (D) H3K9me2 levels and distribution at the indicated genes in MEFs and DCs. The gene fragments associated with H3K9me2 were identified and quantified by ChIP-Seq analysis. Y-axes represent the number of reads per million mapped reads. (E) Abundance of H3K9me2 at the *Ifnβ* promoter in mouse and human cells of various types (left and right, respectively). The levels of H3K9me2 at the *Ifnβ* promoters in different cells types were evaluated by ChIP-qPCR analysis. H3K9me2 was normalized to total histone H3 levels. Data are representative of two independent experiments. Card. Myoc., cardiac myocyte; Neurobl., neuroblastoma; BMDM, BM-derived macrophage; BMDC, BM-derived DC; pDC, splenic pDC; cDC, splenic conventional DC; HLF, human lung fibroblast; MoDC, monocyte-derived DC. Error bars are SD. Data are representative of two independent experiments. (F) Expression of G9a, GLP, H3K9me2, and total H3 in WT MEFs and splenic DCs. The expression of the indicated proteins was determined by Western blotting of nuclear extracts. Lamin B serves as a loading control. M.W., molecular weight. Data are representative of at least three independent experiments.

translocation of phosphorylated transcription factors IRF3 and IRF7, along with NF-κB and AP1, which bind to the *Ifnβ* promoter and initiate IFN gene transcription (Agalioti et al., 2000; Panne et al., 2007). The possible role of increased signaling downstream of pathogen-sensing receptors as the cause for increased production of IFN by plasmacytoid DCs (pDCs) is indicated by stably elevated basal levels of the key IFN-stimulating transcription factor IRF7 in these cells (Honda et al., 2005). At the next step of *Ifnβ* gene activation, acetylation of histones H3 at lysine 9 and lysine 14 and H4 at lysine 8 within the nucleosome encompassing the *Ifnβ* promoter results in the recruitment of CBP-Pol II holoenzyme, nucleosome remodeling by the SWI/SNF complex, recruitment of TFIID, and ultimately transcription of *Ifnβ* (Agalioti et al., 2002).

The functional importance of histone acetylation at the *Ifnβ* gene has been supported by studies that show increased IFN expression in cells treated with histone deacetylase inhibitors or by synthetic antagonists of the acetylated histone interaction with the BET family of transcriptional regulators (Shestakova et al., 2001; Nicodeme et al., 2010). Lysine acetylation of histones requires that lysine residues be free from other forms of posttranslational modification, in particular lysine methylation (Wang et al., 2008). Di- or tri-methylation of H3K9 is capable of preventing activation of gene expression not only passively, by prohibiting acetylation, but also actively, by recruiting transcriptional repressors of the HP1 family (Nakayama et al., 2001; Fischle et al., 2003). Therefore, it is plausible that the levels of H3K9me2/3 at IFN and ISG promoters may contribute to the cell type–specific differences in IFN and ISG expression.

Here, we present data that reveal H3K9 di-methylation as an epigenetic determinant of IFN and ISG expression by cells of various types. We describe a reverse correlation between H3K9me2 occupancy at IFN and ISG promoters and the ability of cells to express these genes. In mice and men, di-methylation of H3K9 is catalyzed by the G9a/GLP enzymatic complex, where G9a is essential for the catalytic function and stability of the complex (Tachibana et al., 2005). We demonstrate that ablation or pharmacological suppression of G9a and ensued deficiency in euchromatic H3K9me2 converts nonprofessional IFN-producing cells into potent IFN and ISG expressers and renders them resistant to viral infection.

RESULTS AND DISCUSSION

"Natural" H3K9me2 deficiency at Type I IFN and ISGs in DCs

Di-methylation of lysine 9 of histone H3 (H3K9me2) is widely linked to transcriptional repression of euchromatic genes and heterochromatic gene silencing (Peters et al., 2003). Although gene transcription is largely governed by upstream signals that recruit transcription factors, the abundance of H3K9me2 at individual gene promoters, including those of IFN and ISGs, could be a limiting factor in what ultimately determines the likelihood of transcription. We speculated that developmentally predetermined and/or signal-controlled H3K9me2 at *Ifnα/β* promoters could contribute to cell type–specific differences in IFN and possibly ISG expression. In agreement with this model, we found significantly lower levels of H3K9me2 at IFN and ISG promoters in splenic DCs as compared with mouse embryonic fibroblasts (MEFs), which have been used as an example of "nonprofessional" IFN-expressing cells. In MEFs, H3K9me2 occupies the entirety of *Ifnβ* as well as the *Mx1* ISG (Fig. 1 A). The pattern of H3K9me2 occupancy of the *Ifnβ* and *Mx1* loci is similar in DCs. However, the gene-specific levels of H3K9me2 in these cells are significantly lower than in MEFs (Fig. 1 A). Similar to the *Ifnβ* and *Mx1* loci, *Ifnα4* and ISG *Ifit1* were nearly depleted of H3K9me2 in DCs (unpublished data). Collectively, H3K9me2 enrichment around the promoters of >300 ISGs (Schoggins et al., 2011) was much lower in DCs than in MEFs, highlighting this difference of epigenetic patterning of antiviral genes in two cell types (Fig. 1 B). Overall, H3K9me2 levels were also low at the promoters of many known proinflammatory genes, including LPS-inducible genes (Fig. 1 C; Ramirez-Carrozzi et al., 2009; Nicodeme et al., 2010). This finding points to "natural" H3K9me2 depletion as an epigenetic hallmark of proinflammatory genes. However, in our studies we choose to focus on poly I:C–induced ISGs as a representative group of genes involved in inflammatory responses. The low abundance of H3K9me2 at IFN and ISGs in DCs is not a consequence of auto- and/or paracrine DC stimulation by IFN as supported by similarly low levels of H3K9me2 at IFN and ISGs promoters in WT and IFNαR1$^{-/-}$ DCs (Fig. 1 A). Reduced levels of H3K9me2 at IFN and ISG promoters in DCs are also associated with a relative enrichment of H3K4me3 at these loci (Fig. 1 B). The latter histone mark is indicative of transcriptionally poised and/or actively transcribed genes (Bernstein et al., 2002). In contrast to IFN and ISGs, neuron- or liver-specific *Nsg1* or *Alb* genes, which are silent in both DCs and MEFs, display equally high levels of H3K9me2 (Fig. 1 D, top). Accordingly, both cell types lacked H3K9me2 at highly expressed housekeeping genes such as *Hprt* or *Gapdh* (Fig. 1 D, bottom).

Discordances in H3K9me2 levels at *Ifnβ* and ISG promoters could also be extended to other cell types. In mice, BM-derived macrophages and DCs, as well as ex vivo isolated splenic plasmacytoid and conventional DCs, showed lower H3K9me2 levels at the *Ifnβ* promoter as compared with MEFs, cardiac myocytes, or neuroblastoma cells. (Fig. 1 E, left). Moreover, the disparity in H3K9me2 levels between DCs and MEFs was conserved between mice and humans, as indicated by high and low levels of H3K9me2 at the *Ifnβ* promoter in human fibroblasts and monocyte-derived DCs, respectively (Fig. 1 E, right).

The mechanism of the locus-specific differences in H3K9me2 levels between DCs and MEFs is not known. DCs express G9a and GLP at slightly lower levels compared with MEFs (Fig. 1 F). However, similar global levels of H3K9me2 in DCs and MEFs (Fig. 1 F), as well as equally high H3K9me2 levels at silent gene promoters in both cell types (Fig. 1 D), suggest equal capacity of DCs and MEFs to catalyze H3K9me2. Therefore, the difference in H3K9me2 levels at IFN and ISG loci in DCs and MEFs might reflect differences in cell type–specific targeting of IFN and ISG loci by G9a/GLP and/or by H3K9me2 demethylases.

G9a deficiency converts MEFs into potent IFN- and ISG-expressing cells

The low levels of H3K9me2 in DCs pointed to a potential role of natural loss of this modification in regulation of IFN and ISG expression. According to this model, removal of H3K9me2 from the *Ifnβ* locus could result in phenotypic conversion of MEFs into DC-like IFN producers. In lieu of naturally low H3K9me2 levels at *Ifnβ*, we expected that

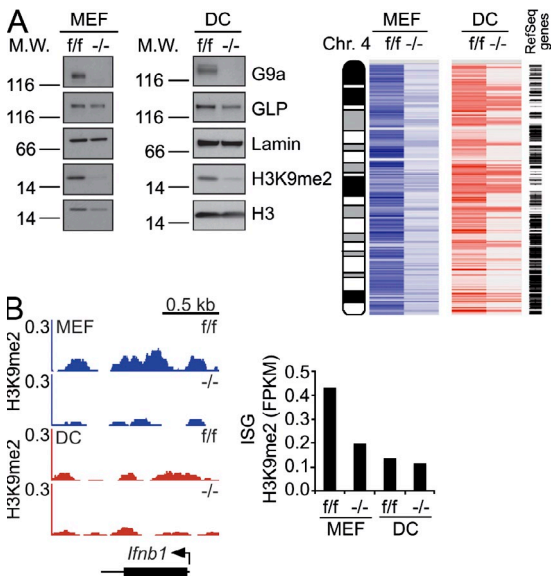

Figure 2. Differential impact of G9a deficiency on H3K9me2 at *Ifnβ* and ISGs in MEFs and DCs. (A, left) The expression levels of G9a, GLP, and H3K9me2 in control (f/f) or G9a deficient (−/−) cells were measured by Western blotting. Lamin B and Histone H3 serve as loading controls. (A, right) The heat map shows distribution and levels of H3K9me2 along chromosome 4 in G9a$^{f/f}$ and G9a$^{-/-}$ MEFs and DCs as determined by ChIP-Seq. A condensed map of RefSeq genes is to the right. (B) Impact of G9a deficiency on H3K9me2 at the *Ifnb1* (left) and ISG loci (right) in MEFs and DCs. H3K9me2 distribution and levels at the *Ifnb1* locus in MEFS or splenic DCs were determined by ChIP-Seq analysis. The mean FPKM values of H3K9me2 levels at ISG promoters in G9a$^{f/f}$ and G9a$^{-/-}$ MEFs and DCs were quantified by ChIP-Seq. Data are representative of two independent experiments for MEFs and one experiment for DCs.

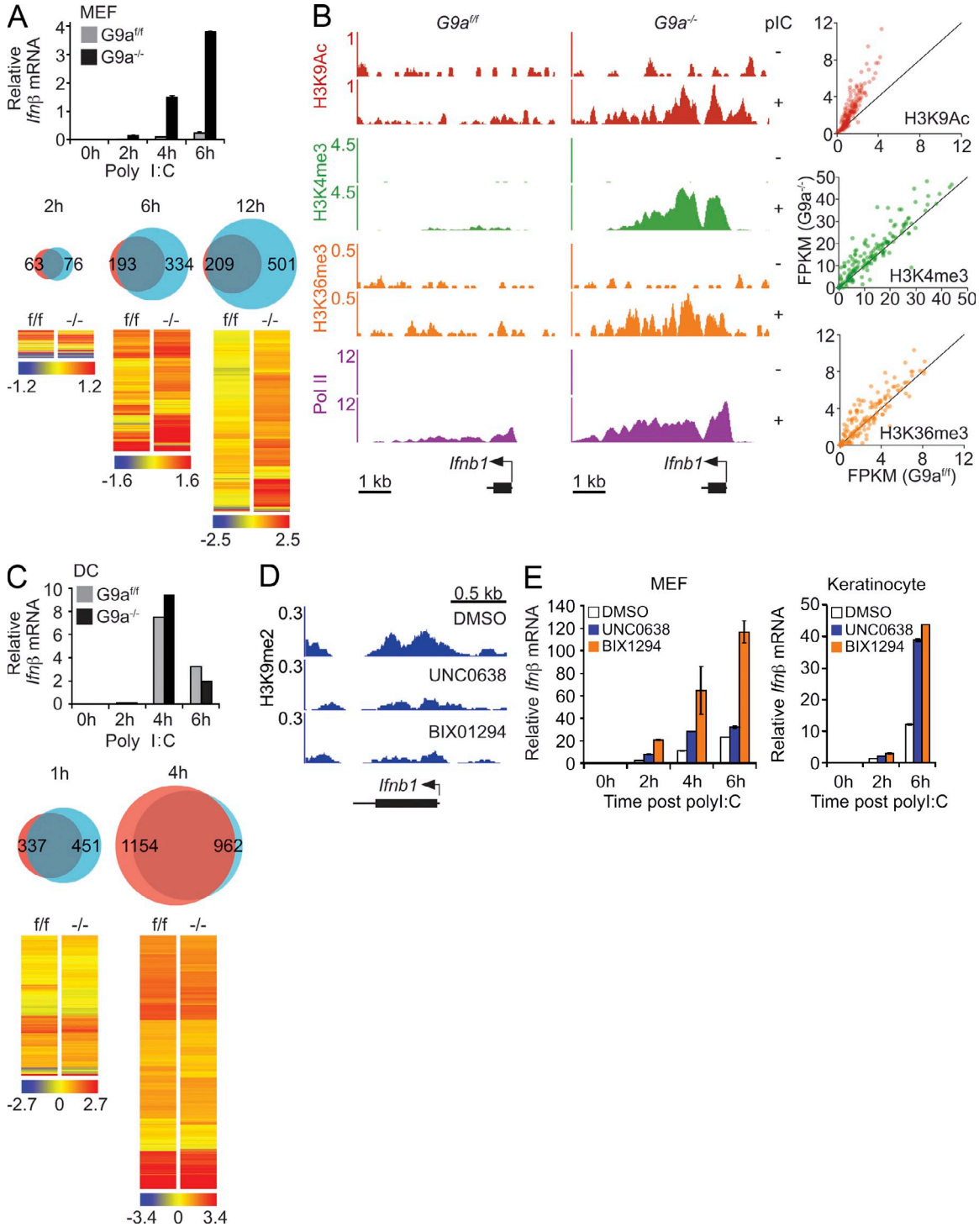

Figure 3. G9a silences *Ifnβ* and IFN-inducible gene expression in fibroblasts. (A) G9a$^{f/f}$ and G9a$^{-/-}$ MEFs were stimulated with poly I:C and *Ifnβ* mRNA levels were determined by qPCR (top). The number and levels of genes in control and G9a-deficient MEFs treated with poly I:C were determined by microarray analysis (bottom). Venn diagrams show the differences in the number of genes that were up-regulated more than twofold in G9a$^{f/f}$ and G9a$^{-/-}$ MEFs. Red, G9a$^{f/f}$; blue, G9a$^{-/-}$. The hierarchical clustered heat maps show expression of the greater than twofold poly I:C–induced genes in G9a$^{-/-}$ as compared with G9a$^{f/f}$ MEFs. Color bar represents $\log_2$ scale of raw signal values for each time point. Data represent triplicate samples. (B) Abundance of the chromatin marks associated with active gene transcription at *Ifnb1* (left) and ISG (right) loci. The distribution and levels of epigenetic marks representing active transcription at *Ifnb1* were measured by ChIP-Seq in G9a$^{f/f}$ and G9a$^{-/-}$ MEFs before and after poly I:C stimulation. Scatter plots display differential abundance of transcription-associated histone marks at poly I:C–induced genes 6 h after stimulation. X- and y-axes are FPKM values for epigenetic marks in G9a$^{f/f}$ and G9a$^{-/-}$ MEFS 6 h after stimulation. (C) G9a$^{f/f}$ and G9a$^{-/-}$ splenic DCs were stimulated with poly I:C and *Ifnβ*

H3K9me2 deficiency in DCs would not have a large impact on gene expression. To study the impact of G9a deficiency on IFN and ISG expression in MEFs, the *G9a* gene was conditionally inactivated by tamoxifen treatment of ERT2-cre;G9a$^{f/f}$ MEFs. G9a-deficient DCs were isolated from Vav-cre;G9a$^{f/f}$ mice, where expression of the Vav1 promoter-driven Cre resulted in G9a inactivation within the hematopoietic lineage.

Deficiency of the G9a gene in MEFs or DCs resulted in loss of G9a protein and global reduction of euchromatic H3K9me2 levels in MEFs and DCs (Fig. 2 A, left). Genome-wide analysis of H3K9me2 distribution, exemplified by the pattern of H3K9me2 abundance along chromosome 4, shows nearly complete loss of H3K9me2 at most genes in DCs and MEFs, except loci that are likely to reside within heterochromatin (Fig. 2 A, right). These results show the essential role of G9a in catalyzing H3K9me2 in DCs in a fashion that has been reported previously for G9a-deficient cells of other lineages (Tachibana et al., 2002; Peters et al., 2003; Rice et al., 2003). However, the consequences of G9a deficiency on IFN and ISGs differed significantly between these cell types. In MEFs, deficiency in G9a drastically reduced the amount of H3K9me2 at *Ifnβ* and ISG promoters to DC-like levels (Fig. 2 B). Because DCs already had naturally low levels of H3K9me2 at *Ifnβ* and ISGs, lack of G9a had little additional impact on this histone modification at these gene promoters. (Fig. 2 B).

Deficiency in G9a and associated loss of H3K9me2 had little impact on basal gene expression in either MEFs or DCs (unpublished data). However, there was a significant and selective impact of G9a deficiency on IFN and ISG expression in MEFs upon poly I:C stimulation. Triggering of G9a-deficient MEFs with poly I:C resulted in significantly stronger and faster up-regulation of *Ifnβ* as compared with WT MEFs (Fig. 3 A, top). In addition, more poly I:C–induced genes were expressed at higher levels in G9a-deficient MEFs as compared with poly I:C–treated control MEFs (Fig. 3 A, bottom; and Table S1). This impact of G9a deficiency was highly gene specific, as mutant MEFs did not display any significant changes in the pattern and levels of the genes that are not involved in the poly I:C response (Table S1). With the exception of six genes, including *Il15* and *Il6*, the expression levels of non-ISG proinflammatory genes were similar in WT and G9a-deficient MEFs (unpublished data). Earlier studies by Ramirez-Carrozzi et al. (2009) revealed several genetic and epigenetic determinants of transcriptional dynamics of proinflammatory genes in macrophages. It is plausible that the differential H3K9me2 contribution to poly I:C–induced ISGs or other proinflammatory gene activation reflects a unique feature of the transcriptional network involved in ISG activation.

The augmented up-regulation of *Ifnβ* and ISGs in G9a-deficient MEFs was associated with a signal-dependent enrichment of transcription-associated marks such as H3K9Ac, H3K4me3, H3K36me3, and Pol II at *Ifnβ* and ISG promoters (Fig. 3 B). Contrary to MEFs, deficiency of G9a in DCs had little additional impact on already robust poly I:C–induced *Ifnβ* and ISG expression (Fig. 3 C).

The positive impact of G9a deficiency on IFN and ISG expression was reproduced by suppression of G9a enzymatic activity (Kubicek et al., 2007; Vedadi et al., 2011). Treatment of MEFs with either BIX1294 or UNC0638 G9a inhibitors lead to reduction of H3K9me2 at the *Ifnβ* locus, as well as an increase in poly I:C–induced *Ifnβ* expression in a fashion similar to G9a-deficient cells (Fig. 3, D and E). Furthermore, inhibition of G9a resulted in enhanced *Ifnβ* expression not only in MEFs but also in poly I:C–stimulated primary mouse keratinocytes (Fig. 3 E).

Enhanced poly I:C–induced IFN and ISG expression in the absence of G9a suggested a key role of G9a-mediated H3K9me2 in the regulation of IFN and ISG promoter accessibility to signal-induced transcription factors. Several lines of evidence support a chromatin-dependent role of G9a in regulation of *Ifnβ* and ISG expression. Deficiency of G9a did not affect poly I:C–induced phosphorylation of IRF3 as evident from appearance of the phosphorylated IRF3 species at 6 h after stimulation (unpublished data). Additionally, a nonchromatinized plasmid-based *Ifnβ* promoter displayed equally strong activity in both mutant and control cells (unpublished data). The levels of STAT1 phosphorylation and activation of a reporter ISG, which carries a STAT-dependent ISRE sequence, were similar in IFN-treated G9a-deficient and control cells (unpublished data). These data ruled out any significant contribution of G9a to signaling processes upstream of IFN-inducing and IFN-induced transcriptional networks. Instead, we found that G9a determines the outcome of the IFN expression even under conditions of excessive transcription factor function. Expression of a constitutively active IRF3 in MEFs resulted in higher *Ifnβ* expression in G9a-deficient as compared with control MEFs (unpublished data).

Previous findings had implicated G9a in the regulation of *Ifnβ* expression by the transcriptional suppressor Blimp1 (Keller and Maniatis, 1991; Gyory et al., 2004). According to the data, binding of G9a to Blimp1 was important for termination of *Ifnβ*

mRNA levels were determined by qPCR. The number and levels of genes in control and G9a-deficient splenic DCs treated with poly I:C were determined by microarray analysis (bottom). Venn diagrams show the number of genes that were up-regulated more than twofold in G9a$^{f/f}$ and G9a$^{-/-}$ DCs. Red, G9a$^{f/f}$; blue, G9a$^{-/-}$. The hierarchical clustered heat maps show expression of the greater than twofold poly I:C–induced genes in G9a$^{-/-}$ as compared with G9a$^{f/f}$ MEFs. Color bar represents $\log_2$ scale of raw signal values for each time point. Data represent duplicate samples. (D) WT MEFS were treated with pharmacological inhibitors of G9a, UNC0638 (1 µM), or BIX1294 (1 µM) for 7 d. The abundance and distribution of H3K9me2 was determined by ChIP-Seq. Y-axes represent the number of reads per million mapped reads. (E) MEFs or primary mouse keratinocytes were treated with DMSO, or with G9a inhibitors BIX1294 and UNC0638 for 7 d. Control or inhibitor-treated cells were stimulated with poly I:C and *Ifnβ* mRNA levels were determined by qPCR. Data are representative of three independent experiments. Error bars are SD.

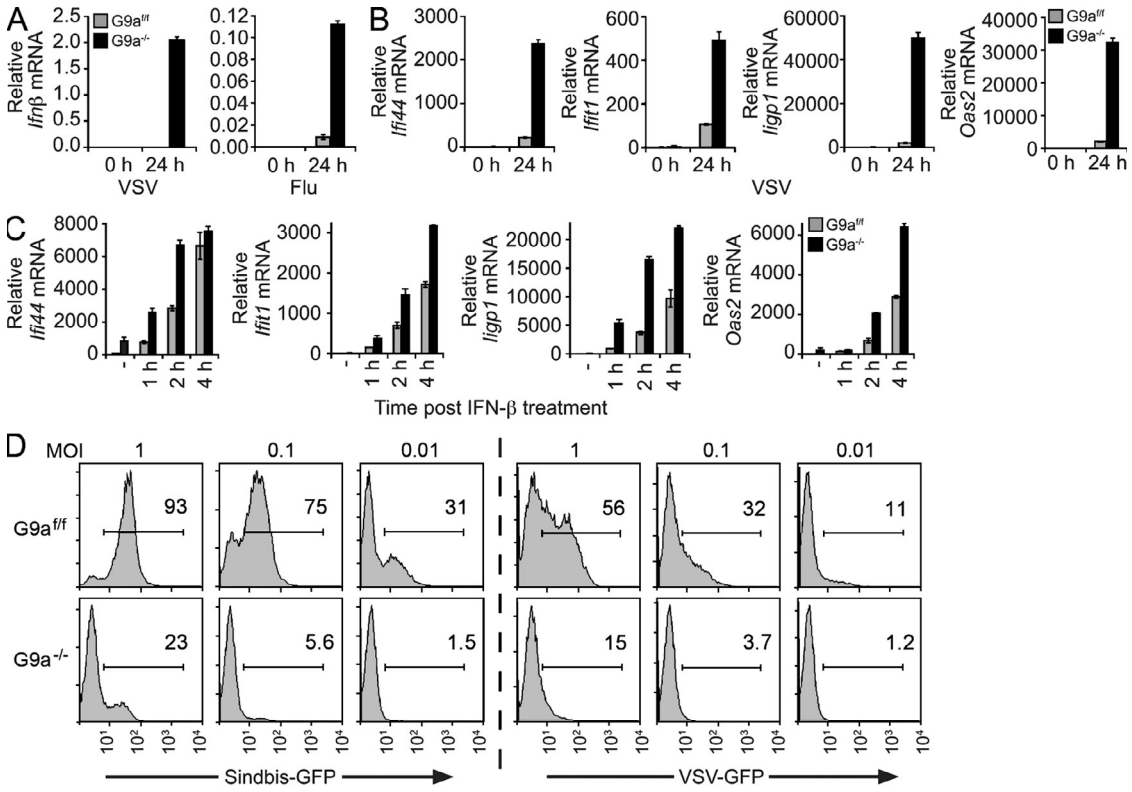

Figure 4. Deficiency of G9a in MEFs enhances resistance to viral infection. (A) G9a$^{f/f}$ and G9a$^{-/-}$ MEFs were infected with VSV (MOI 0.01) or influenza A (MOI 1), followed by the analysis of *Ifnβ* mRNA expression levels by qPCR at 0 and 24 h after infection. (B) G9a$^{f/f}$ or G9a$^{-/-}$ MEFs were infected with VSV (MOI 0.01), followed by the analysis of *Ifi44*, *Ifit1*, *Iigp1*, and *Oas2* mRNA (ISGs) by qPCR at 0 and 24 h after infection. (C) MEFs were stimulated with 500 U/ml recombinant IFN-β and expression of ISGs was determined by qPCR. Untreated is denoted as −. (D) G9a$^{f/f}$ and G9a$^{-/-}$ MEFs were infected with VSV or Sindbis viruses expressing GFP at the indicated MOIs. The infected cells were identified by flow cytometry at 14 h after infection by GFP fluorescence. The histograms show the levels of GFP expression, as well as frequencies, of infected GFP-positive cells. Data (A–D) are representative of at least three independent experiments. Error bars are SD.

gene expression. Theoretically, this mechanism may contribute to enhanced IFN mRNA expression in the absence of G9a. However, we found no evidence for the role of Blimp1 in regulation of IFN and ISG expression in MEFs. Conditional ablation of the *Blimp1* gene in MEFs derived from Blimp1$^{f/f}$ mice (Ohinata et al., 2005) had no impact on either basal or poly I:C–induced *Ifnβ* transcription (unpublished data). Therefore, the previously described G9a-Blimp1 association cannot contribute to enhanced IFN expression in G9a deficient fibroblasts.

Enhanced resistance to viral infection in the absence of G9a

Enhanced poly I:C–stimulated gene expression in G9a$^{-/-}$ MEFs indicated a potential regulatory role of G9a and H3K9me2 in cell susceptibility to viral infection. In G9a-deficient MEFs, *Ifnβ* and ISG expression were greatly enhanced in response to vesicular stomatitis virus (VSV) or influenza A (Fig. 4, A and B). The heightened antiviral gene response reflects both increased production of *Ifnβ* and augmented responsiveness of ISGs to *Ifnβ* stimulation. Incubation of mutant and control MEFs with equal amounts of recombinant IFN-β resulted in higher ISG expression in G9a-deficient MEFs (Fig. 4 C). Enhancement of antiviral gene expression rendered G9a$^{-/-}$ MEFs resistant to viral infection. Sindbis or VSV viruses, engineered to express GFP to monitor the frequency of infected cells and relative viral replication levels per cell, could not replicate in G9a-deficient cells as efficiently as in control cells (Fig. 4 D).

We provide evidence for a key role of G9a-mediated H3K9me2 in the regulation of IFN expression and antiviral transcriptional program. We established a reverse correlation between the abundance of H3K9me2 at IFN and ISG promoters with the scope and amplitude of activation of these genes. We also show that H3K9me2 deficiency, which follows G9a genetic ablation or pharmacological suppression, boosts IFN and ISG expression in MEFs to high levels and renders MEFs highly resistant to viral infection. Importantly, stimulation of MEFs or other cell types with poly I:C or viruses does not dramatically change the abundance of H3K9me2 at the IFN or ISG promoters (unpublished data). Therefore, the amount of H3K9me2 at IFN or ISG could be viewed as a new developmentally installed lineage-specific epigenetic determinant

of the IFN-driven innate response. Mechanistically, abundance of H3K9me2 within a nucleosome that carries two histone H3 molecules defines the number of nucleosomes and, hence, gene alleles that could be driven into active transcription by signal-induced histone H3 acetylation. Therefore, our data suggest that the ability of DCs to express high levels of IFN, as compared with MEFs, is based on a developmentally determined relatively higher number of IFN and ISG alleles accessible for transcriptional activation.

The key role of H3K9me2 in the IFN response raises a question of the role of H3K9me2 methylating and demethylating enzymes in inflammatory and autoimmune diseases that are rooted in increased IFN production. In this context, it would be important to determine the abundance of H3K9me2 at IFN and ISG promoters in monocytes from patients with systemic lupus erythematosus who display heightened levels of IFN expression (IFN signature) in the absence of stimulation (Pascual et al., 2006).

MATERIALS AND METHODS

Mice. C57BL/6 mice were obtained from Charles River. $G9a^{f/f}$ and $Glp^{f/f}$ mice were described previously (Sampath et al., 2007; Schaefer et al., 2009). Rosa26-ER^{T2}-Cre mice were provided by T. Ludwig (Columbia University, New York, NY). Vav-cre mice were obtained from The Jackson Laboratory. $IFNAR1^{-/-}$ mice were obtained from B&K Universal Ltd. All mice were bred onto a C57BL/6 background. Mice were housed under specific pathogen-free conditions and experimental protocols were approved by the Rockefeller University Institutional Animal Care and Use Committee.

Cells. MEFs were generated from day 12.5 or 13.5 embryos from $G9a^{f/f}$; Rosa26-ER^{T2}-Cre mice and immortalized with SV40-LTA before deletion of G9a was induced with 4-OH Tamoxifen. MEFs were cultured in DME with 10% FBS, L-Glutamine, penicillin-streptomycin, and 2-mercaptoethanol. Cardiac myocytes were isolated from day 6 embryonic stem cells expressing α-MHC and grown in puromycin as described previously (Kolossov et al., 2006). N2A neuroblastoma cells were cultured in DME supplemented with 5% FBS, 50% Opti-MEM, and penicillin-streptomycin. To induce expansion of splenic DCs, C57BL/6, $G9a^{fl/fl}$ mice, $G9a^{fl/fl}$;Vav-Cre mice, and $IFN\alpha R1^{-/-}$ mice were subcutaneously injected with 5×10^6 B16-Flt3L cells. 2 wk later, splenic DCs were enriched for the $CD11c^+$ population using CD11c MACS beads (Miltenyi Biotec). pDCs were enriched with mPDCA-1 MACS beads (Miltenyi Biotec). pDCs ($B220^+CD11b^-CD11c^+$mPDCA-1^+) and conventional DCs ($B220^-CD11b^+CD11c^+$mPDCA-1^-) were further purified by cell sorting (FACSAria; BD). BM-derived DCs were cultured and differentiated for 8 d in RPMI supplemented with 10% FBS, L-Glutamine, penicillin-streptomycin, sodium pyruvate, Hepes, 2-mercaptoethanol, and 100 ng/ml mFlt3-L (R&D systems). BM-derived macrophages were cultured and differentiated for 6 d in DME containing 10% FBS, L-Glutamine, penicillin-streptomycin, 5 ng/ml IL-3 (PeproTech), and 5 ng/ml MCSF-1 (PeproTech). Primary mouse keratinocytes were maintained in E medium with 15% FBS and 50 μM $CaCl_2$ (low Ca^{2+} medium). Human lung fibroblasts (CC-2512; Lonza) were subcultured in supplemented FGM-2 culture media (BulletKit CC-3132; Lonza). For generation of human monocyte-derived DCs, blood samples collected into heparin-containing tubes were diluted twofold in Dulbecco's PBS (DPBS) and separated on a Ficoll-plaque gradient (density 1.077; GE Healthcare). The interphase was transferred to a fresh tube and diluted to 40 ml using DPBS and centrifuged twice for 5 min at 200 *g* to reduce platelet contamination. Monocytes were further purified using a monocyte isolation kit (Miltenyi Biotec). To obtain DCs, monocytes were plated in culture media (RPMI-1640, 10% FCS, 2 mM L-Glutamine, 100 U/ml penicillin, and 100 μg/ml streptomycin) supplemented with 30 ng/ml GM-CSF (R&D Systems) and 20 ng/ml IL-4 (R&D Systems). Cells were fed every other day with the cytokine cocktail and the DCs were harvested by day 7. Human biological samples were obtained from healthy donors for research use. The samples were sourced ethically and collected and used in accordance with the terms of the informed consents and under Hertfordshire Research Ethics Committee approval.

ChIP. Cells were fixed with 1% formaldehyde and fixation was stopped by addition of glycine. ChIP and preparation of samples for ChIP-Seq was performed as previously described (Lee et al., 2006; Nicodeme et al., 2010). Quantitative PCR was performed with a Light Cycler 480 (Roche) using SYBR green for detection of real-time transcripts. Standard curves were generated using input DNA to normalize for differences in primer efficiencies. Data are represented as the amount of ChIP DNA/Input DNA or ChIP DNA associated with Histone H3.

Analysis of ChIP-Seq. Samples were amplified onto flow cells using a standard cluster station (Illumina) per manufacturer protocol. Cluster kits used were version 4 single read cluster amplification kits. Samples were sequenced on the GAIIx platform (Illumina) for 36 cycles using version 4 sequencing kits, and raw sequencing data were processed using the onboard SCS/RTA software version 2.6 yielding 36 bp reads. Sequencing reads were aligned to the mouse genome (NCBI37/mm9) using Bowtie (Langmead et al., 2009). Reads were kept if they aligned with two errors or less over the 36 bp read length and did not align to more than one location in the genome.

Normalization of $G9a^{f/f}$ and $G9a^{-/-}$ MEF and DC H3K9me2 ChIP-Seq. As the distribution of reads between the WT and $G9a^{f/f}$ cells will reflect markedly different regions and levels of enrichment of H3K9me2, the typical method of normalization based purely on the number of sequencing reads obtained would not provide a useful means of equilibrating enrichment signals, and a method based on Major Satellite repeat enrichment was used. Quantitative PCR (qPCR) data indicated increases in signal for H3K9me2-associated Major Satellite enrichment in $G9a^{f/f}$ cells with respect to WT cells in both MEFs and DCs. Repeat analysis was performed by aligning reads to the rodrep.ref repeat file from RepBase15.01, allowing two errors over 36 bp. The number of reads aligning to Major Satellite sequence was tabulated for WT and $G9a^{f/f}$ cells. Using the qPCR data, a target value was obtained that reflected the number of Major Satellite–associated reads expected for $G9a^{f/f}$ (WT multiplied by qPCR-observed increase). The ratio of observed-to-expected counts was calculated for MEF and DC datasets and used to adjust enrichment values and browser visualizations.

ChIP-Seq enrichment (FPKM). To determine the enrichment of H3K9me2, H3K4me3, H3K9Ac, and H3K36me3, the total number of reads aligning to the specified region of interest was calculated and reported as fragments per kilobase of region per million mapped reads (FPKM). This normalizes the enrichment values based on read number and length of region of interest. Regions of interest were: ±1 kb from the TSS for H3K9me2; ±3 kb for H3K4me3 and H3K9Ac; and full transcript length for H3K36me3. RefSeq data downloaded from the University of California, Santa Cruz table browser was used.

Per-gene profiles. Browser tracks were displayed using the Integrative Genome Viewer, and made using the igvtools count function set for 100 bp extensions in the 3′ direction and either 5 bp or 25 bp windows. ChIP-Seq data are accessible through Gene Expression Omnibus, accession no. GSE22102.

RNA isolation, reverse transcription, and qPCR. RNA was isolated with the RNeasy mini kit (QIAGEN). RNA was reverse transcribed using Superscript III (Invitrogen). qPCR was performed using SYBR green and products were quantified with a standard curve. Gene expression was displayed relative to *Tbp*.

Microarray analysis. 1 μg of total RNA from two (DC) or three (MEF) samples per group was used to prepare biotin-labeled RNA using Ambion Illumina TotalPrep RNA Amplification kit (Applied Biosystems) and hybridized to Illumina MouseRef-8 v2.0 expression BeadChip kits. The chips were scanned using a BeadArray Reader (Illumina) followed by analysis using Genespring (Affymetrix). The raw expression data were quality assessed

and subjected to background adjustment and normalization. The individual gene expression levels were compared by using an unpaired Student's *t* test ($P < 0.05$) and by pairwise comparison. The microarray datasets are available in the Gene Expression Omnibus under the accession no. GSE24826.

Stimulations and transfections. MEFs were transfected with 2 μg/ml poly I:C with Lipofectamine 2000 (Invitrogen) according to the manufacturer's instructions. Reporter constructs were transfected with $CaPO_4$. The IFN-β reporter was provided by T. Taniguchi (University of Tokyo, Tokyo, Japan). The ISRE reporter was obtained from Invitrogen. DCs were directly stimulated with 10 μg/ml poly I:C.

Viruses and viral infection. Stocks of GFP-expressing VSV (designated VSV-GFP M51R titered by serial dilution on Vero cells), as well as influenza A (Puerto Rico/8/34 [H1N1], amplified in 8-d-old embryonated chicken eggs and titered by plaque assay on Madin-Darby canine kidney cells), were provided by A. Garcia-Sastre (Mount Sinai School of Medicine, New York, NY). WT VSV Indiana serotype (San Juan), originally a gift from M. Schlesinger (Washington University School of Medicine, St. Louis, MO), was grown and titered on BHK-21 cells as previously described (Bick et al., 2003). GFP-expressing Sindbis virus TE/5′2J-GFP, which expresses GFP from a duplicated subgenomic promoter, was previously described (Frolova et al., 2002). Viral stocks were produced by electroporation of BHK-21 cells with in vitro–generated RNA transcripts from plasmid pTE/5′2J-GFP and titered on BHK-21 cells by plaque assay as previously described (Bick et al., 2003). MOI (multiplicity of infection) calculations were based on the titers obtained in the cell types mentioned previously. MEFs were incubated with virus in PBS supplemented with 1% FBS, calcium and magnesium for 1 h at 37°C. Virus was removed and replaced with fresh media. This was considered time 0 h. For flow cytometric analysis of GFP expression, cells were fixed with 4% paraformaldehyde before analysis on a FACSCalibur flow cytometer (BD).

Antibodies. H3 (ab1791), H3K9me2 (ab1220), H3K9Ac (ab4441), H3K36me3 (ab9050), total Pol II (ab5408), and Pol II S5 (ab5153) antibodies were all obtained from Abcam. H3K4me3 was from Millipore (17614). Phospho-IRF3 (4947) and phospho-STAT1 (9171) were from Cell Signaling Technology. GLP (BO422) was from Perseus Proteomics. IRF3 (51–3200) was from Invitrogen, and STAT1 (610185) was from BD. The G9a antibody was described previously (Sampath et al., 2007).

G9a/GLP inhibitors. BIX1294 and UNC0638 were obtained from Sigma-Aldrich. Both inhibitors were used at 1 μM. Cells were incubated with inhibitor for 7 d and the media was replenished with fresh inhibitor every 2 d.

Online supplemental material. Table S1 shows genes that were upregulated more than twofold in $G9a^{f/f}$ and $G9a^{-/-}$ MEFs stimulated with poly I:C at 2, 6, and 12 h. Online supplemental material is available at http://www.jem.org/cgi/content/full/jem.20112343/DC1.

We are grateful to Tada Taniguchi, Adolfo Garcia-Sastre, Dan Stetson, and David Levy for many valuable reagents. We thank Srihari Sampath for the initial discussions about the role of G9a in antiviral responses; Angela Santana for technical assistance; the Genomics Resource Center for performing microarray and sequencing; the Flow Cytometry Resource Center for cell sorting; and Rebecca Rizzo for editorial assistance.

T.C. Fang was supported by the Irvington Institute Fellowship Program of the Cancer Research Institute. A. Tarakhovsky was supported by National Institutes of Health grant R21AI077018 and the Starr Cancer Consortium. M.R. MacDonald and C.M. Rice were supported by the Greenberg Medical Research Institute, the Starr Foundation, and National Institutes of Health grant R01 AI091707. A. Stienen was supported by the Medical School RWTH Aachen University.

I. Rioja, V. Parravicini, R.K. Prinjha, and K. Lee are employees of GlaxoSmithKline. Research support, including ChIP-Seq analysis, supplies, and other expenses, was provided by GlaxoSmithKline.

Submitted: 4 November 2011
Accepted: 14 February 2012

REFERENCES

Agalioti, T., S. Lomvardas, B. Parekh, J. Yie, T. Maniatis, and D. Thanos. 2000. Ordered recruitment of chromatin modifying and general transcription factors to the IFN-beta promoter. *Cell*. 103:667–678. http://dx.doi.org/10.1016/S0092-8674(00)00169-0

Agalioti, T., G. Chen, and D. Thanos. 2002. Deciphering the transcriptional histone acetylation code for a human gene. *Cell*. 111:381–392. http://dx.doi.org/10.1016/S0092-8674(02)01077-2

Barchet, W., M. Cella, and M. Colonna. 2005. Plasmacytoid dendritic cells—virus experts of innate immunity. *Semin. Immunol*. 17:253–261. http://dx.doi.org/10.1016/j.smim.2005.05.008

Bernstein, B.E., E.L. Humphrey, R.L. Erlich, R. Schneider, P. Bouman, J.S. Liu, T. Kouzarides, and S.L. Schreiber. 2002. Methylation of histone H3 Lys 4 in coding regions of active genes. *Proc. Natl. Acad. Sci. USA*. 99:8695–8700. http://dx.doi.org/10.1073/pnas.082249499

Bick, M.J., J.W. Carroll, G. Gao, S.P. Goff, C.M. Rice, and M.R. MacDonald. 2003. Expression of the zinc-finger antiviral protein inhibits alphavirus replication. *J. Virol*. 77:11555–11562. http://dx.doi.org/10.1128/JVI.77.21.11555-11562.2003

Diebold, S.S., M. Montoya, H. Unger, L. Alexopoulou, P. Roy, L.E. Haswell, A. Al-Shamkhani, R. Flavell, P. Borrow, and C. Reis e Sousa. 2003. Viral infection switches non-plasmacytoid dendritic cells into high interferon producers. *Nature*. 424:324–328. http://dx.doi.org/10.1038/nature01783

Fischle, W., Y. Wang, S.A. Jacobs, Y. Kim, C.D. Allis, and S. Khorasanizadeh. 2003. Molecular basis for the discrimination of repressive methyl-lysine marks in histone H3 by Polycomb and HP1 chromodomains. *Genes Dev*. 17:1870–1881. http://dx.doi.org/10.1101/gad.1110503

Frolova, E.I., R.Z. Fayzulin, S.H. Cook, D.E. Griffin, C.M. Rice, and I. Frolov. 2002. Roles of nonstructural protein nsP2 and Alpha/Beta interferons in determining the outcome of Sindbis virus infection. *J. Virol*. 76:11254–11264. http://dx.doi.org/10.1128/JVI.76.22.11254-11264.2002

Gyory, I., J. Wu, G. Fejér, E. Seto, and K.L. Wright. 2004. PRDI-BF1 recruits the histone H3 methyltransferase G9a in transcriptional silencing. *Nat. Immunol*. 5:299–308. http://dx.doi.org/10.1038/ni1046

Honda, K., H. Yanai, H. Negishi, M. Asagiri, M. Sato, T. Mizutani, N. Shimada, Y. Ohba, A. Takaoka, N. Yoshida, and T. Taniguchi. 2005. IRF-7 is the master regulator of type-I interferon-dependent immune responses. *Nature*. 434:772–777. http://dx.doi.org/10.1038/nature03464

Keller, A.D., and T. Maniatis. 1991. Identification and characterization of a novel repressor of beta-interferon gene expression. *Genes Dev*. 5:868–879. http://dx.doi.org/10.1101/gad.5.5.868

Kolossov, E., T. Bostani, W. Roell, M. Breitbach, F. Pillekamp, J.M. Nygren, P. Sasse, O. Rubenchik, J.W. Fries, D. Wenzel, et al. 2006. Engraftment of engineered ES cell–derived cardiomyocytes but not BM cells restores contractile function to the infarcted myocardium. *J. Exp. Med*. 203:2315–2327. http://dx.doi.org/10.1084/jem.20061469

Kubicek, S., R.J. O'Sullivan, E.M. August, E.R. Hickey, Q. Zhang, M.L. Teodoro, S. Rea, K. Mechtler, J.A. Kowalski, C.A. Homon, et al. 2007. Reversal of H3K9me2 by a small-molecule inhibitor for the G9a histone methyltransferase. *Mol. Cell*. 25:473–481. http://dx.doi.org/10.1016/j.molcel.2007.01.017

Kumagai, Y., O. Takeuchi, H. Kato, H. Kumar, K. Matsui, E. Morii, K. Aozasa, T. Kawai, and S. Akira. 2007. Alveolar macrophages are the primary interferon-alpha producer in pulmonary infection with RNA viruses. *Immunity*. 27:240–252. http://dx.doi.org/10.1016/j.immuni.2007.07.013

Langmead, B., C. Trapnell, M. Pop, and S.L. Salzberg. 2009. Ultrafast and memory-efficient alignment of short DNA sequences to the human genome. *Genome Biol*. 10:R25. http://dx.doi.org/10.1186/gb-2009-10-3-r25

Lee, T.I., S.E. Johnstone, and R.A. Young. 2006. Chromatin immunoprecipitation and microarray-based analysis of protein location. *Nat. Protoc*. 1:729–748. http://dx.doi.org/10.1038/nprot.2006.98

Nakayama, J., J.C. Rice, B.D. Strahl, C.D. Allis, and S.I. Grewal. 2001. Role of histone H3 lysine 9 methylation in epigenetic control of heterochromatin assembly. *Science*. 292:110–113. http://dx.doi.org/10.1126/science.1060118

Nicodeme, E., K.L. Jeffrey, U. Schaefer, S. Beinke, S. Dewell, C.W. Chung, R. Chandwani, I. Marazzi, P. Wilson, H. Coste, et al. 2010. Suppression of inflammation by a synthetic histone mimic. *Nature*. 468:1119–1123. http://dx.doi.org/10.1038/nature09589

Ohinata, Y., B. Payer, D. O'Carroll, K. Ancelin, Y. Ono, M. Sano, S.C. Barton, T. Obukhanych, M. Nussenzweig, A. Tarakhovsky, et al. 2005. Blimp1 is a critical determinant of the germ cell lineage in mice. *Nature*. 436:207–213. http://dx.doi.org/10.1038/nature03813

Panne, D., T. Maniatis, and S.C. Harrison. 2007. An atomic model of the interferon-beta enhanceosome. *Cell*. 129:1111–1123. http://dx.doi.org/10.1016/j.cell.2007.05.019

Pascual, V., L. Farkas, and J. Banchereau. 2006. Systemic lupus erythematosus: all roads lead to type I interferons. *Curr. Opin. Immunol.* 18:676–682. http://dx.doi.org/10.1016/j.coi.2006.09.014

Peters, A.H., S. Kubicek, K. Mechtler, R.J. O'Sullivan, A.A. Derijck, L. Perez-Burgos, A. Kohlmaier, S. Opravil, M. Tachibana, Y. Shinkai, et al. 2003. Partitioning and plasticity of repressive histone methylation states in mammalian chromatin. *Mol. Cell*. 12:1577–1589. http://dx.doi.org/10.1016/S1097-2765(03)00477-5

Pietras, E.M., S.K. Saha, and G. Cheng. 2006. The interferon response to bacterial and viral infections. *J. Endotoxin Res.* 12:246–250. http://dx.doi.org/10.1179/096805106X118799

Ramirez-Carrozzi, V.R., D. Braas, D.M. Bhatt, C.S. Cheng, C. Hong, K.R. Doty, J.C. Black, A. Hoffmann, M. Carey, and S.T. Smale. 2009. A unifying model for the selective regulation of inducible transcription by CpG islands and nucleosome remodeling. *Cell*. 138:114–128. http://dx.doi.org/10.1016/j.cell.2009.04.020

Rice, J.C., S.D. Briggs, B. Ueberheide, C.M. Barber, J. Shabanowitz, D.F. Hunt, Y. Shinkai, and C.D. Allis. 2003. Histone methyltransferases direct different degrees of methylation to define distinct chromatin domains. *Mol. Cell*. 12:1591–1598. http://dx.doi.org/10.1016/S1097-2765(03)00479-9

Sampath, S.C., I. Marazzi, K.L. Yap, S.C. Sampath, A.N. Krutchinsky, I. Mecklenbräuker, A. Viale, E. Rudensky, M.M. Zhou, B.T. Chait, and A. Tarakhovsky. 2007. Methylation of a histone mimic within the histone methyltransferase G9a regulates protein complex assembly. *Mol. Cell*. 27:596–608. http://dx.doi.org/10.1016/j.molcel.2007.06.026

Schaefer, A., S.C. Sampath, A. Intrator, A. Min, T.S. Gertler, D.J. Surmeier, A. Tarakhovsky, and P. Greengard. 2009. Control of cognition and adaptive behavior by the GLP/G9a epigenetic suppressor complex. *Neuron*. 64:678–691. http://dx.doi.org/10.1016/j.neuron.2009.11.019

Schoggins, J.W., S.J. Wilson, M. Panis, M.Y. Murphy, C.T. Jones, P. Bieniasz, and C.M. Rice. 2011. A diverse range of gene products are effectors of the type I interferon antiviral response. *Nature*. 472:481–485. http://dx.doi.org/10.1038/nature09907

Shestakova, E., M.T. Bandu, J. Doly, and E. Bonnefoy. 2001. Inhibition of histone deacetylation induces constitutive derepression of the beta interferon promoter and confers antiviral activity. *J. Virol.* 75:3444–3452. http://dx.doi.org/10.1128/JVI.75.7.3444-3452.2001

Stetson, D.B., and R. Medzhitov. 2006. Type I interferons in host defense. *Immunity*. 25:373–381. http://dx.doi.org/10.1016/j.immuni.2006.08.007

Tachibana, M., K. Sugimoto, M. Nozaki, J. Ueda, T. Ohta, M. Ohki, M. Fukuda, N. Takeda, H. Niida, H. Kato, and Y. Shinkai. 2002. G9a histone methyltransferase plays a dominant role in euchromatic histone H3 lysine 9 methylation and is essential for early embryogenesis. *Genes Dev.* 16:1779–1791. http://dx.doi.org/10.1101/gad.989402

Tachibana, M., J. Ueda, M. Fukuda, N. Takeda, T. Ohta, H. Iwanari, T. Sakihama, T. Kodama, T. Hamakubo, and Y. Shinkai. 2005. Histone methyltransferases G9a and GLP form heteromeric complexes and are both crucial for methylation of euchromatin at H3-K9. *Genes Dev.* 19:815–826. http://dx.doi.org/10.1101/gad.1284005

Trinchieri, G. 2010. Type I interferon: friend or foe? *J. Exp. Med.* 207:2053–2063. http://dx.doi.org/10.1084/jem.20101664

Vedadi, M., D. Barsyte-Lovejoy, F. Liu, S. Rival-Gervier, A. Allali-Hassani, V. Labrie, T.J. Wigle, P.A. Dimaggio, G.A. Wasney, A. Siarheyeva, et al. 2011. A chemical probe selectively inhibits G9a and GLP methyltransferase activity in cells. *Nat. Chem. Biol.* 7:566–574. http://dx.doi.org/10.1038/nchembio.599

Wang, Z., C. Zang, J.A. Rosenfeld, D.E. Schones, A. Barski, S. Cuddapah, K. Cui, T.Y. Roh, W. Peng, M.Q. Zhang, and K. Zhao. 2008. Combinatorial patterns of histone acetylations and methylations in the human genome. *Nat. Genet.* 40:897–903. http://dx.doi.org/10.1038/ng.154